



Introduction

Niobium alloyed titanium aluminides are a promising candidate for material substitution in high temperature applications. Their balanced mechanical performance together with the good oxidation resistance and the low density make them an attractive basis for further alloy development.

The alloy design could be supported by a better understanding of the underlying micromechanical mechanisms. In the two-phase intermetallic alloys a large variety of deformation mechanisms can be activated and their interaction is very diverse.

Considered microstructures

Due to their involved phase diagram, titanium aluminides can produce a large variety of microstructures. A fully lamellar microstructure evolves in the case of slow cooling. The so called convoluted microstructure^[Wu2004] results from high cooling rates which lead to massive transformation ($\alpha \rightarrow \gamma$). By appropriate heat treatment precipitation of alpha from massively transformed gamma ($\gamma \rightarrow \alpha \rightarrow \alpha_2$) will take place.

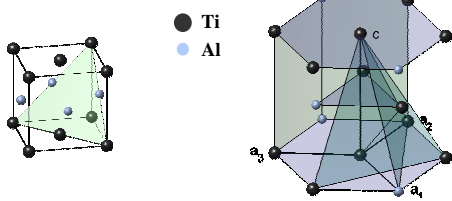


Fig. 1: Crystal structures of the face-centered-tetragonal $L1_0$ -ordered gamma-TiAl phase and the hexagonal DO_{19} -ordered alpha2-Ti3Al phase: TiAl can deform on {111} planes in directions $b=\frac{1}{2}\langle 110 \rangle$ (ordinary dislocations), $b=\langle 101 \rangle$ (super dislocations) or $(a/6)\langle 11\bar{2} \rangle$ (twinning). For Ti3Al basal ("a"), prismatic ("c") and pyramidal ("a+c") slip systems can be activated.

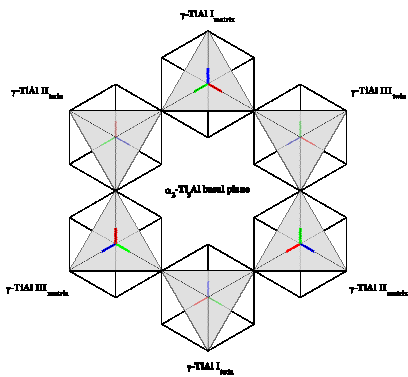


Fig. 2: Gamma TiAl in the lamellar structure occurs in six distinct orientational variants. Opposite variants in the figure are in true twin relation. The Blackburn orientation relationship with the alpha2 basal plane is also shown.

Crystal plasticity model

A phenomenological crystal plasticity formulation for slip and twinning on the deformation systems is used ^[Kalidindi1992]. Any imposed deformation of the material is partitioned into shear contributions from the individual deformation systems of the respective phases.

$$\dot{\gamma}^\alpha = \dot{\gamma}_0 \left| \frac{\tau^\alpha}{s^\alpha} \right|^{1/m} \text{sign}(\tau^\alpha) \quad \dot{s}^\alpha = \sum_\beta q^{\alpha\beta} h^{(\beta)} \left| \dot{\gamma}^\beta \right|$$

Constitutive relations for both phases are implemented into a material subroutine for use with a finite element solver. Twinning deformation is implemented as a uni-directional slip system. The slip and twinning systems can be assigned different strengths and hardening behavior to account for various influences on critical resolved shear stress evolution.

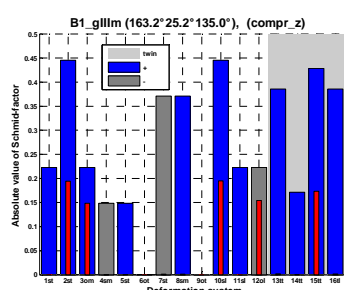


Fig. 3: The magnitude of schmidfactors for the deformation systems of the single orientational variant gamma-III-matrix in orientation B1. The red bars show the amount of shear on the activated systems after 66 increments of deformation.

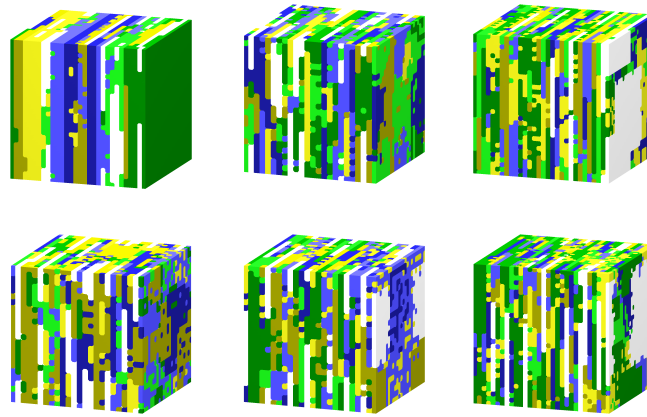


Fig. 4: Artificially generated lamellar microstructures: The colouring scheme represents the different orientational variants (white: alpha2; others: gamma-I-matrix, gamma-I-twin, gamma-II-matrix, gamma-II-twin, gamma-III-matrix, gamma-III-twin)

Generation of the RVE

A cellular automaton is used to generate 3D microstructures of the lamellar type (see Fig. 4). This method enables efficient generation of realistic microstructures with regard to phase volume fractions, spatial arrangement and size distribution of the different phases. Additionally the resulting microstructures are "grown" under periodic boundary conditions and therefore are well suited for representative volume element (RVE) calculations under periodic boundary conditions.

Thanks to the flexible growth dynamics of the cellular automaton, also characteristic features of the convoluted microstructure can be captured by defining an appropriate transition function.

RVE calculations

Finite element models are built from the 3D phase distribution resulting from the cellular automaton. Each finite element is consisting of only one phase. Periodic boundary conditions (see Fig. 5) are used for the calculations.

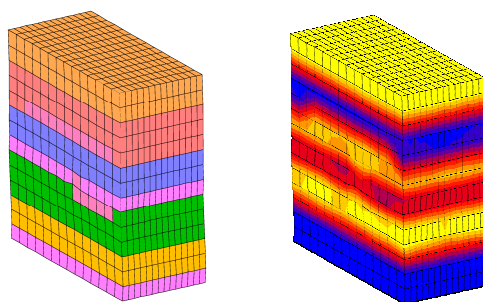


Fig. 5: Finite element model for RVE calculations. The nonhomogeneous distribution of shear on slip system $(\bar{1}11)[\bar{1}0\bar{1}]$ is shown for a model of a lamellar PST-crystal.

Volume averaging is used to extract global stress-strain curves from the heterogeneous stress and strain fields and the shear contributions per phase.

Anisotropy in lamellar microstructures

Polysynthetically twinned crystals of TiAl exhibit strong plastic anisotropy^[Inui1992]. This is supposed to be mainly caused by the alpha2 lamellae which drastically confine the dislocation movement in gamma phase perpendicular to the lamellar planes. If shear is allowed to act in parallel to the lamellar plane the overall response is ductile and soft. When the tensile or compressive stresses act along or perpendicular to the lamellar planes the response will be much harder. This hard and soft modes of deformation are also responsible for the small ductility of fine grained material with a lamellar microstructure. In the crystal plasticity model this is incorporated by assigning different hardening behaviour to deformation systems acting along the lamellar plane (longitudinal mode) or perpendicular to it (transversal mode).

Coherency stresses

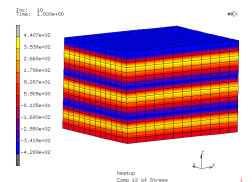
Finer lamellar arrangements result in higher coherency stresses of several ten MPa and even more.

Coherency stresses are generated during the solid state phase transformation. The ordered phases obey a Blackburn orientation relationship which aligns the (111) plane of the gamma-phase with the basal plane of alpha2. Due to lattice misfit at the interface between the alpha2 and the orientational variants of gamma, significant coherency stresses can develop depending on the processing history of the alloy^[Grinfeld1998, Appel1999].

Coherency stresses are incorporated in the model by applying the transformation strains for each phase in an initial loading step before the actual deformation of the RVE takes place.

In the case of the lamellar structure the misfit stresses are expected to be of higher relevance than for the massive transformation microstructure which contains a smaller amount of interphase area, i.e. larger microstructural constituents.

Fig. 6: Coherency stresses in a lamellar stack of gamma variants. The calculation shows results for linear elasticity without plastic relaxation.



Experimental validation

In the past much experimental work has been done on the characterisation of the anisotropic flow-behavior of PST-crystals. Besides such uniaxial testing also nano-indentation experiments in individual phases of the microstructure have been reported^[Göken2001]. These experiments are of special interest, because the in-situ mechanical properties of the microstructural constituents cannot be measured by experiments on single phase material.

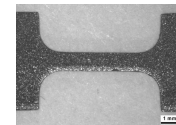


Fig. 7: Small sized sample for mechanical testing in an in-situ SEM-EBSD system. The gauge length is 4 mm and width is 1 mm.

Tensile testing of small sized samples, in combination with strain mapping by digital image correlation, will be done on directionally solidified material, to capture the interaction of anisotropic lamellar grains

Conclusion

Micromechanical modeling of near-gamma TiAl generates insight and quantitative information regarding the stress and strain state in the microstructural elements. Based on experimental input, it can lead to quantitative statements on the microstructure properties relation. The presented crystal plasticity approach is, in addition to experimental work, a tool to clarify the interplay between the deformation mechanisms in a complex material like Ti-Al-Nb.

In this work emphasis is put on the microstructure properties relation in two different kinds of microstructures of the same composition.

Acknowledgements

Support by the EU FP6 project IMPRESS (Intermetallic Materials Processing in Relation to Earth and Space Solidification) is gratefully acknowledged.

Stefan Schulz is thanked for the introduction to his efficient cellular automaton software framework.

References:

- X. Wu, D. Hu, M.H. Loretto: J. Mater. Sci. 39 (2004) pp. 3935-3940
- S. Kalidindi, C. Bronkhorst, L. Anand: J. Mech. Phys. Solids 40 (1992) pp. 537-569
- H. Inui, M.H. Oh, A. Nakamura, M. Yamaguchi: Acta Mater 40 (1992) pp. 3095-3104
- M.A. Grinfeld, P.M.Hazzledine, B. Shoykhet, D.M. Dimiduk: Metall. Mater. Trans. A 29 (1998) pp.937-942
- F. Appel, U. Christoph: Intermetallics 7 (1999) pp.1173-1182
- M. Göken, M. Kempf, W. D. Nix: Acta mater. 49 (2001) pp. 903-911